An *In Situ* X-ray Tomography Study on the Stress Corrosion Behavior of a Ni-Based Single-Crystal Superalloy

HAOYI NIU, FANGCHENG ZHENG, HAO WANG, CHENGLU LIU, RENGENG LI, XUEWEN LI, HAO WU, QING LIU, and GUOHUA FAN

The present study was devoted to investigating the stress corrosion behavior of Ni-based single-crystal superalloys using *in situ* three-dimensional X-ray tomography. The dynamics of a total of 169 cavities were tracked *in situ* for representative statistics. Our results demonstrated that the growth rate of the cavities under stress corrosion conditions was correlated with their size and spatial distribution, which provides new insights for preventing premature cavity coarsening through the tailoring of the cavity.

https://doi.org/10.1007/s11661-022-06925-6

NI-BASED single-crystal superalloys have been extensively used as turbine blades due to their excellent creep performance, fatigue resistance, and antioxidation.[1–4] During alloy solidification, casted cavities were frequently generated[5–7] because (i) the merging of the secondary dendrite arms diminishes the liquid supply in the direction perpendicular to the primary dendrite stem. These cavities are often formed at the intersections of primary dendrites and dendrite arms or within the interior of dendrites,[8,9] and (ii) thermal shrinkage promotes solidification of residual liquid between dendrites, which leaves room for pore formation.[9] A large number of investigations have focused on the influence of shrinkage cavities on the mechanical characteristics of Ni-based single-crystal superalloys in recent years.[10–13] It is generally known that shrinkage cavities easily evolve into early cracks if loaded.[14] Additionally, the fatigue and creep properties of Ni-based superalloys are primarily affected by the size, shape, and distribution of casted cavities.[15–18] For instance, the creep resistance of superalloys below 1000 °C can be greatly enhanced by reducing the cavity size and density through hot isostatic pressing.[19]

The aforementioned research was mainly focused on the impact of shrinkage cavities on the tensile, fatigue, and creep characteristics of Ni-based single-crystal superalloys. Nevertheless, turbine blades were subjected to a large centrifugal stress derived from high-speed rotation upon service.[20–22] At the same time, Ni-based single-crystal blades may operate in an acidic environment, such as chloride ions, and suffer from corrosion damage caused by the gas combustion products and the deleterious pollution of the atmosphere.[23–28] The actual working conditions of Ni-based single-crystal turbine blades are analogous to the stress corrosion environment. As a major casting defect, shrinkage porosity is one of the common sources for crack initiation, which significantly degrades the mechanical properties of the superalloy. Therefore, it is crucial to investigate the influence of cavity defects on the mechanical performance of Ni-based superalloys under stress corrosion conditions. Traditional characterization techniques generally provide a two-dimensional view of the size and distribution of shrinkage cavities. In recent years, rapidly developed high-resolution X-ray computed tomography has enabled the identification of micron-scale cavities,[29–32] which makes it serving as a more suitable method to study the porosity effect. In the present study, *in situ* X-ray tomography was performed to study the stress corrosion behavior of Ni-based single-crystal superalloys and thus to further elucidate the growth kinetics of casted cavities at the sample surface and in the sample interior.

HAOYI NIU is with the College of Materials Science and Engineering, Chongqing University, Chongqing 400030, P.R. China. FANGCHENG ZHENG, HAO WANG, CHENGLU LIU, RENGENG LI, XUEWEN LI, and HAO WU are with the Key Laboratory for Light-weight Materials, Nanjing Tech University, Nanjing 210009, P.R. China. Contact e-mail: hwu@njtech.edu.cn QING LIU is with the College of Materials Science and Engineering, Chongqing University and also with the Key Laboratory for Light-weight Materials, Nanjing Tech University. GUOHUA FAN is with the Key Laboratory for Light-weight Materials, Nanjing Tech University and also with the Advanced Materials Research Institute, Yangtze Delta, Suzhou 215100, P.R. China. Contact e-mail: ghfan@njtech.edu.cn
Manuscript submitted August 23, 2022; accepted November 15, 2022.
Article published online December 26, 2022

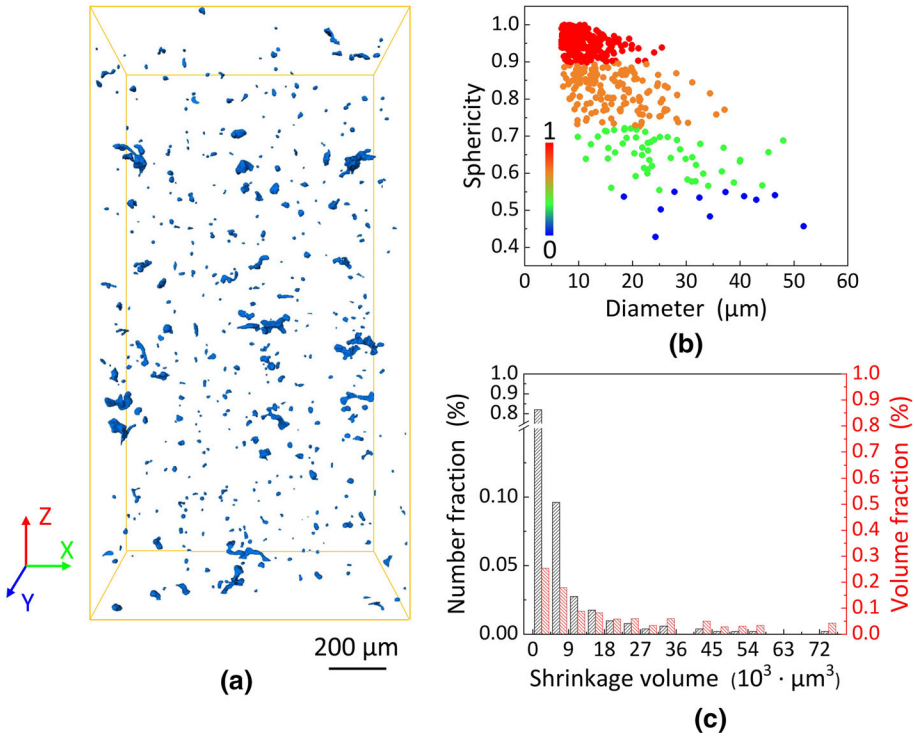

Fig. 1—Shrinkage cavities of as-received Ni-based single-crystal superalloys. (*a*) Three-dimensional rendering; (*b*) sphericity distribution; and (*c*) number and volume frequency.

The nominal composition of the selected Ni-based single-crystal superalloys in the present study was Ni–5Cr–1.0Ti–5.8Al–1.0Mo–11.8W–9.0Co–1.5Nb–1.0V (all in wt pct, unless otherwise stated). Stress corrosion samples were extracted from the single-crystal rod along the [001] crystal orientation by a medium wire cutting machine with dimensions of 3 mm (length) × 1 mm (width) × 1 mm (thickness). The samples were then polished with 200 to 2000 SiC sandpapers and polished on microfiber cloth with 1.0 to 0.05 μm diamond polishing agent to remove surface defects. The stress corrosion test was performed by a Zeiss Xradia Versa 620 X-ray microscope equipped with a stress corrosion device, as shown in electronic supplementary Figure S1. The X-ray energy was 150 keV, and the power was 23 W. The corrosive solution was composed of 280 g/L $FeCl_3$ plus 120 g/L HCl. A tensile stress of 450 MPa was always applied. Image processing, 3D rendering, and quantitative analysis of the number density, size, and sphericity of cavities were performed using Avizo software.

The microstructure of the as-received Ni-based single-crystal superalloy is shown in electronic supplementary Figure S2. Dark shrinkage cavities were clearly observed on both sides of the dendrite stem. The formation of such cavities was due to insufficient liquid at the dendrite stem caused by the merging of dendrite arms. Similar cavities were also detected between dendrite arms, or dendrites, as well as at the interaction between dendrites. We then characterized the shrinking cavities by removing the pixel of the matrix. As shown in Figure 1, the shrinkage cavities were uniformly distributed but differed in the equivalent diameter and sphericity. Quantitative statistics indicated that the smaller the size, the larger the sphericity (Figure 1(b)); more specifically, the sphericity of the shrinkage cavities was close to 1 when the equivalent diameter was very small and deviated from the "ideal" sphericity with increasing cavity diameters. It was also found that small cavities were predominated; for example, the number density of cavities with volumes of $< 9 \times 10^3$ μm^3 occupied approximately 90 pct; however, their volume fraction was only 45 pct (Figure 1(c)).

In situ stress corrosion was performed on the Ni-based single-crystal superalloys. Prior to corrosion, typical microstructures, such as dendritic stems, primary dendrites, and secondary dendrites, are presented in Figure 2(a). The sample was then subjected to an acidic corrosive environment for 5 minutes. The morphological characteristics after corrosion are shown in Figure 2(b). Corrosion cracking was frequently observed between the dendrites and secondary dendrites of the single-crystal superalloy since chloride ions can easily access the matrix *via* shrinkage cavities and dendrites. Figure 2(c) indicates the microstructure after stress corrosion for 12 hours. It is visible that the early crack further propagated along the dendrite. In addition, the surface cracking of the sample started to behave inhomogeneously. When the corrosion period was prolonged up to 24 hours, the cracking degree became more severe and almost traversed the whole dendritic arm (Figure 2(d)). For clear visualization, the pixels corresponding to the cracks/voids are colored navy blue in Figure 2(e). We found that the internal shrinkage cavity did not change significantly throughout the stress corrosion process, and the cavities were mostly

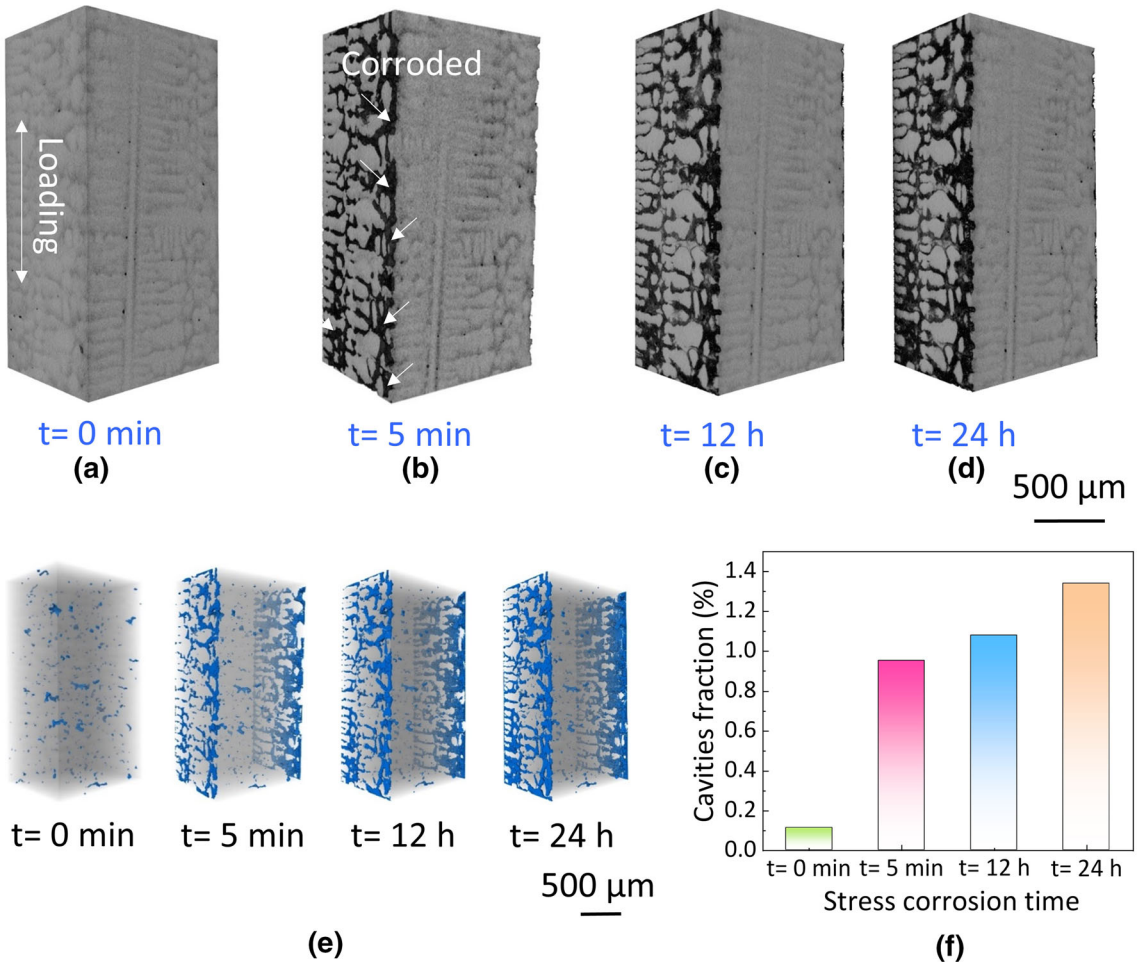

Fig. 2—*In situ* three-dimensional rendering of Ni-based single-crystal superalloys after stress corrosion at (*a*) 0 minute, (*b*) 5 minutes, (*c*) 12 hours, and (*d*) 24 hours. (*e*) The evolution of the cavities and (*f*) quantitative statistics of the cavity volume upon stress corrosion.

spread between the dendritic stem and dendrite arm. The latter implied that the gap between the dendrite stem and dendrite arm served as a corrosion channel, causing local rapid failure. The quantitative statistics in Figure 2(f) also indicated a fast increase in the void fraction with prolonged stress corrosion.

To quantify the evolution of shrinkage cavities during stress corrosion, we separated these shrinkage cavities into internal shrinkage cavities and external surface cavities based on their spatial position. The evolution of several randomly distributed internal cavities upon stress corrosion is shown in Figure 3. Six cavities of interest were selected and marked by red arrows (Figure 3(a)). The kinetic analysis revealed that the internal cavities were not affected during the whole stress corrosion process, even if a long corrosion period of 24 hours was applied, only with a very limited surface deformation. We further evaluated the microdeformation degree of the internal cavities, and no significant deviations in the cavity volume were found after stress corrosion (of the same order of magnitude of merely 5 to 15 $\times$ 10^3 μm^3, see electronic supplementary Figure S3).

We then focused on the evolution of external surface cavities, since they directly touched the corrosive liquid and their kinetics may be fundamentally different from that of the internal cavity. Several representative surface cavities were selected in Figure 4 to elucidate the influence of the corrosion environment. The morphologies of the surface cavities were dramatically changed, even if the sample was etched for only 5 minutes (Figure 4(b)). Further corrosion promoted the connection between the external corrosive liquid and the internal shrinkage cavity so that the corrosive liquid could enter the internal cavity, thereby aggravating the corrosion. In electronic supplementary Figures S4 and S5, we show the three-dimensional geometry of the surface cavity and observe coarsening and interconnection when a cavity is very close to its neighbor.

The aforementioned experimental results pointed out the significant difference in the growth kinetics of internal and surface cavities. In particular, the volume of the internal cavity was slightly varied, while that of surface cavities rapidly increased. Such a deviation may be correlated with the environment they situated, where the surface cavities suffered from the synergetic roles of

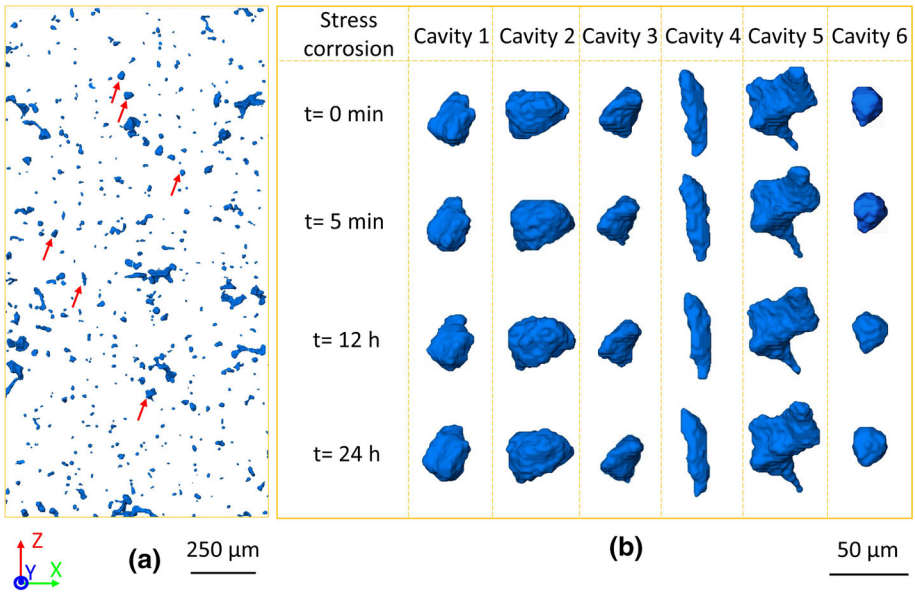

Fig. 3—(*a*) Spatial distribution and (*b*) three-dimensional rendering of the evolution of internal shrinkage cavities under different stress corrosion conditions (Color figure online).

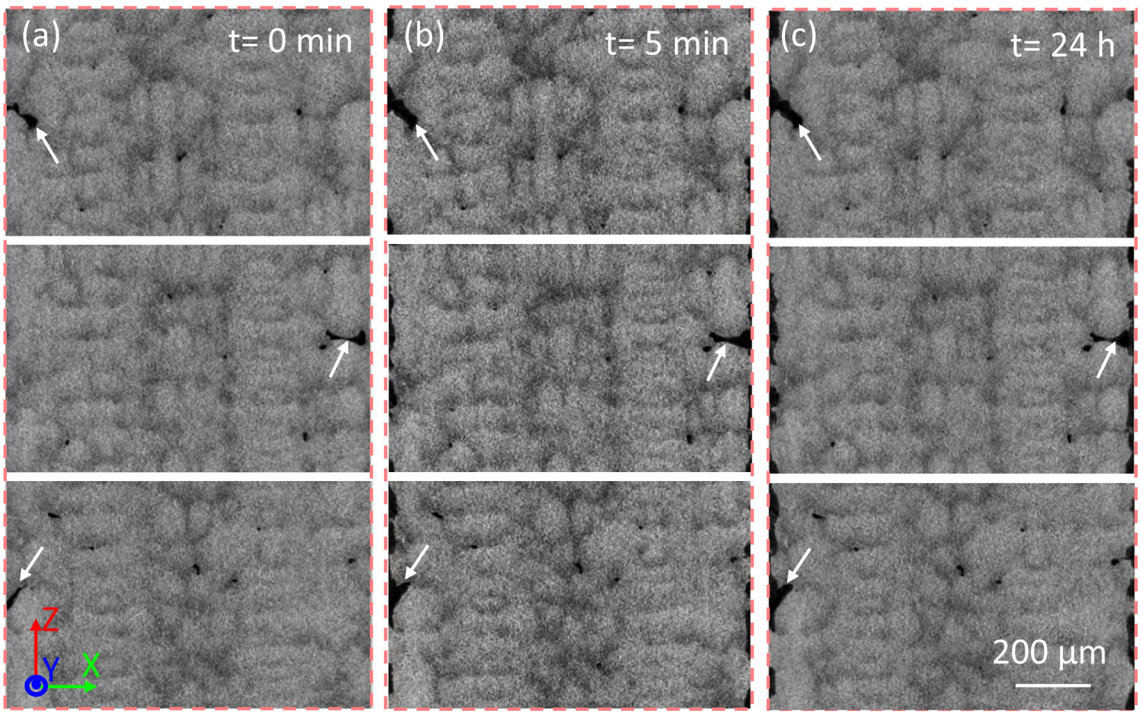

Fig. 4—Two-dimensional slices of shrinkage cavities after stress corrosion at (*a*) 0 minute, (*b*) 5 minutes, and (*c*) 24 hours.

stress and corrosion; however, for the internal cavity, the contribution of the stress is much more important. We further randomly selected a total of 169 cavities to quantify the growth behavior. Figure 5(a) shows that the volume change of internal cavities was several times lower than that of external surface cavities. As an example, the volume change of external small cavities can be as large as > 70 pct, while that of internal cavities was < 10 pct, highlighting the positive effect of the corrosion environment on cavity coarsening. In addition, we elucidated the size-dependent kinetic behavior using the volume change of the cavity normalized by its corresponding initial volume as the vertical coordinate of Figure 5(b). Our quantitative results confirmed that the smaller the cavity, the larger the degree of the volume change. This finding also agrees well with the rapid coarsening of the surface cavity at the initial stress corrosion stage, as shown in Figure 4(b).

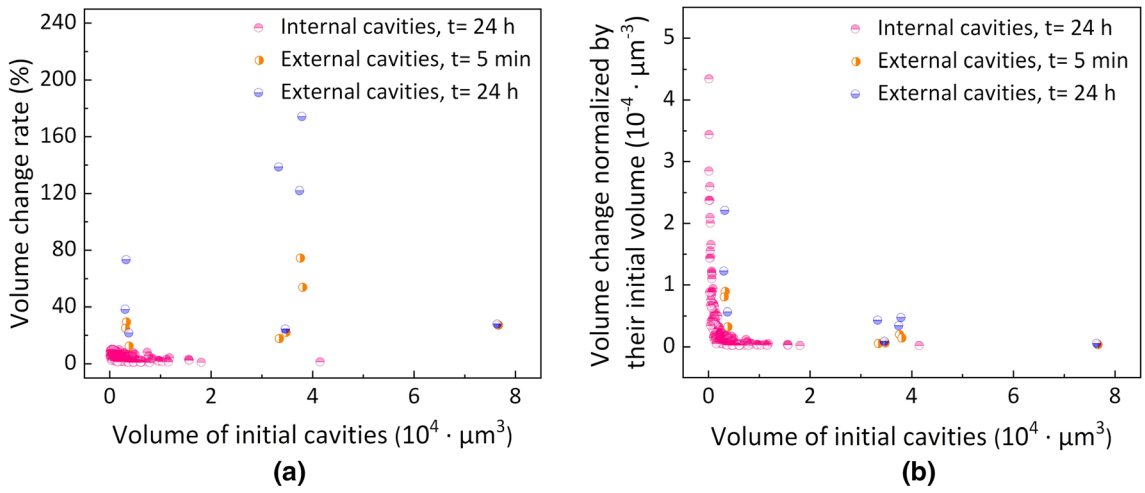

Fig. 5—Quantitative analysis of the influence of the initial cavity volume on (*a*) the volume change and (*b*) the volume change normalized by the corresponding initial cavity volume.

In summary, *in situ* three-dimensional X-ray tomography was employed to investigate the stress corrosion behavior of Ni-based single-crystal superalloys. The growth kinetics of the cavity were closely correlated with its spatial position. Quantitative measurements confirmed that the dynamics of the surface cavity were several times larger than those of internal cavities since the volume change of the surface cavity was substantially accelerated by both the stress and corrosion environment. In addition, the cavity with a small volume exhibited a greater growth tendency. The present study therefore provides insights into protecting the material by tailoring the cavity size and spatial distribution.

ACKNOWLEDGMENTS

This work was financially supported by the National Key Research & Development Plan (Nos. 2021YFA1600702, 2020YFA0405900), National Natural Science Foundation of China (Nos. 52171117, 52001160, 52001161), Natural Science Foundation of Jiangsu Province (Nos. BK20200695, BK20202010), General University Science Research Project of Jiangsu Province (No. 20KJB430011), and State Key Lab of Advanced Metals and Materials (No. 2022-Z19).

CONFLICT OF INTEREST

The authors declare that they have no known competing financial interests or personal relationships that could have appeared to influence the work reported in this paper.

SUPPLEMENTARY INFORMATION

The online version contains supplementary material available at https://doi.org/10.1007/s11661-022-06925-6.

REFERENCES

1. R.C. Reed: *The Superalloys Fundamentals and Applications*, Cambridge University Press, Cambridge, 2006.
2. H. Long, S. Mao, Y. Liu, H. Yang, H. Wei, Q. Deng, Y. Chen, A. Li, Z. Zhang, and X. Han: *Acta Mater.*, 2020, vol. 185, pp. 233–44.
3. M. Zhang, Y. Zhao, Y. Guo, Y. Liu, J. Zhang, Y. Luo, and Z. Yao: *Metall. Mater. Trans. A*, 2022, vol. 53A, pp. 2214–25.
4. Y. Huang, J. Shen, D. Wang, G. Xie, Y. Lu, L. Lou, and J. Zhang: *Metall. Mater. Trans. A*, 2019, vol. 51A, pp. 99–103.
5. J. Lecomte-Beckers: *Metall. Trans. A*, 1988, vol. 19A, pp. 2341–48.
6. Q.Z. Chen, Y.H. Kong, C.N. Jones, and D.M. Knowles: *Scripta Mater.*, 2004, vol. 51, pp. 155–60.
7. X. Li, L. Wang, J. Dong, L. Lou, and J. Zhang: *Metall. Mater. Trans. A*, 2017, vol. 48A, pp. 2682–86.
8. E. Plancher, P. Gravier, E. Chauvet, J.-J. Blandin, E. Boller, G. Martin, L. Salvo, and P. Lhuissier: *Acta Mater.*, 2019, vol. 181, pp. 1–9.
9. Z. Xu, B. Britton, and Y. Guo: *Mater. Sci. Eng. A*, 2021, vol. 806A, p. 140800.
10. H. Buck, P. Wollgramm, A.B. Parsa, and G. Eggeler: *Mat.-wiss. u. Werkstofftech.*, 2015, vol. 46, pp. 577–90.
11. K. Prasad, R. Sarkar, and K. Gopinath: *Mater. Sci. Eng. A*, 2016, vol. 654A, pp. 381–89.
12. A. Epishin and T. Link: *Philos. Mag.*, 2004, vol. 84, pp. 1979–2000.
13. J.-B. le Graverend, J. Adrien, and J. Cormier: *Mater. Sci. Eng. A*, 2017, vol. 695A, pp. 367–78.
14. L. Kunz, P. Lukáš, and R. Konečná: *Int. J. Fatigue*, 2010, vol. 32, pp. 908–13.
15. Z. Zhao, F. Zhang, C. Dong, X. Yang, and B. Chen: *Metall. Mater. Trans. A*, 2020, vol. 51A, pp. 1575–92.
16. W. Jiang, P. Li, W.-X. Yao, S.-S. Rui, H.-J. Shi, and J. Huang: *Int. J. Fatigue*, 2021, vol. 147, p. 106191.
17. B. Ruttert, C. Meid, L. Mujica Roncery, I. Lopez-Galilea, M. Bartsch, and W. Theisen: *Scripta Mater.*, 2018, vol. 155, pp. 139–43.
18. A. Cervellon, J. Cormier, F. Mauget, Z. Hervier, and Y. Nadot: *Metall. Mater. Trans. A*, 2018, vol. 49A, pp. 3938–50.
19. L. Mujica Roncery, I. Lopez-Galilea, B. Ruttert, D. Bürger, P. Wollgramm, G. Eggeler, and W. Theisen: *Adv. Eng. Mater.*, 2016, vol. 18, pp. 1381–87.
20. X. Yao, Q. Ding, X. Zhao, X. Wei, J. Wang, Z. Zhang, and H. Bei: *Mater. Today Nano*, 2022, vol. 17, p. 100152.
21. W. Xia, X. Zhao, L. Yue, and Z. Zhang: *J. Alloys Compd.*, 2020, vol. 819, p. 152954.
22. W. Yang, J. Li, S. Liu, Z. Shi, J. Zhao, and X. Wang: *Trans. Nonferrous Met. Soc. China*, 2019, vol. 29, pp. 558–68.
23. W. Sun, J. Wang, L. Yang, M. Chen, Z. Bao, C. Zheng, S. Zhu, and F. Wang: *Corros. Sci.*, 2019, vol. 161, p. 108187.

24. W. Wang, Y. Cui, R. Liu, L. Liu, and F. Wang: *Corros. Sci.*, 2022, vol. 195, p. 110004.
25. Y. Geng, Y. Mo, H. Zheng, G. Li, and K. Wang: *Corros. Sci.*, 2021, vol. 185, p. 109419.
26. X. Montero, A. Ishida, T.M. Meißner, H. Murakami, and M.C. Galetz: *Corros. Sci.*, 2020, vol. 166, p. 108472.
27. L.N. Zhang and O.A. Ojo: *Metall. Mater. Trans. A*, 2017, vol. 49A, pp. 295–304.
28. M.K. Kumawat, C. Parlikar, M.Z. Alam, and D.K. Das: *Metall. Mater. Trans. A*, 2020, vol. 52A, pp. 378–93.
29. H. Wu and G. Fan: *Prog. Mater. Sci.*, 2020, vol. 113, p. 100675.
30. H. Wu, M. Huang, Q. Li, J. Wu, J. Li, Z. Wang, and G. Fan: *Scripta Mater.*, 2019, vol. 172, pp. 165–70.
31. G. Fan, L. Geng, H. Wu, K. Miao, X. Cui, H. Kang, T. Wang, H. Xie, and T. Xiao: *Scripta Mater.*, 2017, vol. 135, pp. 63–67.
32. Y. Xia, H. Wu, K. Miao, X. Li, C. Xu, L. Geng, H. Xie, and G. Fan: *J. Mater. Sci. Technol.*, 2022, vol. 111, pp. 256–67.